


**Taming convergence in the determinant approach for x-ray excitation spectra**Yufeng Liang<sup>\*</sup> and David Prendergast<sup>†</sup>*The Molecular Foundry, Lawrence Berkeley National Laboratory, Berkeley, California 94720, USA* (Received 30 April 2019; revised manuscript received 14 July 2019; published 9 August 2019)

A determinant formalism in combination with *ab initio* calculations was proposed recently and has paved a way for simulating and interpreting x-ray excitation spectra in condensed-phase systems. The method systematically takes into account many-electron effects in the Mahan-Nozières-De Dominicis (MND) theory, including core-level excitonic effects, the Fermi-edge singularity, shakeup excitations, and wave function overlap effects such as the orthogonality catastrophe, all within a universal framework using many-electron configurations. A heuristic search algorithm was introduced to search for the configurations that are important for defining the x-ray spectral line shape, instead of enumerating them in a brute-force way. The algorithm has proven to be efficient for calculating O *K* edges of transition metal oxides, which converge at the second excitation order (denoted as  $f^{(n)}$  with  $n = 2$ ), i.e., the final-state configurations with two  $e$ - $h$  pairs (with one hole being the core hole). However, it remains unknown how the determinant x-ray spectra converge for general cases and at which excitation order  $n$  should one stop the determinant calculation. Even with the heuristic algorithm, the number of many-electron configurations still grows exponentially with the excitation order  $n$ . In this work we prove two theorems that can indicate the order of magnitude of the contribution of the  $f^{(n)}$  configurations, so that one can estimate their contribution very quickly without actually calculating their amplitudes. The two theorems are based on singular-value decomposition (SVD) analysis, a method that is widely used to quantify entanglement between two quantum many-body systems. We examine the *K* edges of several metallic systems with the determinant formalism up to  $f^{(5)}$  to illustrate the usefulness of the theorems.

DOI: [10.1103/PhysRevB.100.075121](https://doi.org/10.1103/PhysRevB.100.075121)**I. INTRODUCTION**

X-ray spectroscopy has become increasingly important for providing insights into many problems in materials characterization at microscopic scale [1–7], especially in recent times when this area is propelled by the development of light sources enabled by free-electron lasers [8–10]. We consider resonant x-ray excitations, where a core electron of a specific type of atom is promoted into orbitals localized on or near that atomic site, revealing a wealth of information of local chemical environment and electronic structure. The near-edge part of an x-ray absorption spectrum, i.e., a few eVs above onset, is of particular interest, indicating element-specific details of band-edge electronic structure relevant to intriguing physics and chemical processes [3]. The interpretation of x-ray spectra, however, is often a nontrivial task that requires accurate first-principles modeling of both atomic and electronic structure of interest and their associated spectra [11–13]. While the structural properties of a wide range of materials can be mostly captured by density-functional theory (DFT) [14–18], predicting x-ray excited-state spectra in a reliable and efficient manner presents a greater theoretical challenge.

There has been a broad spectrum of theoretical approaches for simulating x-ray excitation spectra. At one extreme, exact diagonalization [19–26] has been applied to rigorously solve the many-electron Hamiltonian. This method represents the

most accurate solutions and is most amendable for localized x-ray excitations that occur within a few atomic orbitals, due to the exponential growth of the many-electron Hilbert space. Wannier down-folding is typically required for reducing the size of the Hamiltonian [21,23] and the Coulomb interaction is usually simplified as an on-site Hubbard  $U$  term. Similar methodology is also employed in the quantum chemistry community within the configuration interaction [27,28] and other post-Hartree-Fock methods [29,30], in which *realistic* Coulomb interactions and superposition of many-electron configurations are considered explicitly in the calculation. Likewise, increasing the size of the excited-state calculation is hindered by the exponential barrier associated with the size of the Hilbert space, although placing restrictions on the active orbital space can mitigate the problem to some extent [31–33]. Due to its rigor, this class of methods can be used for systems with strong electron correlation, but due to its computational inefficiency, it is limited to specific cases such as small molecules [31,33] or clusters [26] and 3*d* metal *L* edges (dominated by localized atomic multiplet effects) [21,25] so far.

At the other extreme, excited-state spectra of condensed phases can be routinely obtained using *ab initio* methods based on DFT and many-body perturbation theory (MBPT), where electron correlation is treated with less rigor but higher efficiency. There are two representative methods. One is the Delta-self-consistent-field ( $\Delta$ SCF) approach [1,11,34,35] that treats the core hole as an external potential, and maps a many-electron excited state to an empty orbital. Many-electron response is taken into account by DFT electronic relaxation,

<sup>\*</sup>yufengliang@lbl.gov, pcbee912@gmail.com<sup>†</sup>dgprendergast@lbl.gov

and then the transition matrix elements are calculated using Fermi's golden rule. In previous formalisms, however, only one-body orbitals are employed for final states, which does not account for proper time ordering of the many-electron processes in x-ray excitations [1,2], leading to possible failures in predicting the intensity of an absorption edge. The other method is the core-level Bethe-Salpeter equation (BSE) [36–38] within MBPT that utilizes the DFT ground state as a zero-order approximation and incorporates many-electron correlations in a *perturbative* manner. A subset of Feynman diagrams generated by the direct and exchange kernels are included to account for *e-h* interactions (excitonic effects), and hence the correct time ordering is retained in this approach. Formulations akin to the BSE are also adopted in linear-response of time-dependent DFT (TDDFT) [39–43], in which exchange-correlation kernels substitute for an *e-h* interaction kernel, or in the corresponding real-time propagation approaches [41,42]. There are many successful application of the  $\Delta$ SCF core-hole approach [11,34,35,44,45] and the core-level BSE [1,38,46] in extended systems, and even in molecules [34] where the Coulomb interaction is not well screened.

### A. Motivations and advantages of the determinant formalism

Following the philosophy of the post DFT methods, we recently proposed a determinant formalism [1,2] for simulating x-ray excitation spectra based on the one-body core-hole approach. In essence, we use a single determinant comprised of Kohn-Sham (KS) orbitals of the unexcited system to approximate the initial state, and a single determinant comprised of KS orbitals of the core-excited system to approximate *each* x-ray excited state. Typically, there is a basis-set transformation of basis set between these two sets of KS orbitals. Transition amplitudes between these determinants, when represented in a common orbital basis, also take the form of determinants of subsets of the orbital transformation matrix. This approach currently describes all states as single determinants. It does not involve configuration interactions among multiple many-electron configurations.

The determinant formalism has three main advantages: First, it provides an exact solution to all the many-electron effects considered within the Mahan-Nozières-De Dominicis (MND) model [47–50], which is beyond the scope of *e-h* attraction in the BSE. These effects include the power-law edge singularity as considered by Mahan using Feynman diagrams [50], and the many-body wave function overlap effect considered by Anderson in the orthogonality catastrophe [51]. In a less dramatic manner, the latter often manifests as *shakeup effects* [52–54], but not edge-rounding effects. Shakeup effects refer to multielectron excitations evident at higher absorption energies which are not explicitly represented in the single electron-hole pair projection of the BSE.

Second, the determinant formalism adopts many-electron configurations in the calculation, and hence provides a conceptually simple picture for understanding x-ray excited states. In the x-ray final-state system, a many-body state is simply a single determinant (single reference) of the occupied KS orbitals. Each excited state is now mapped to its composite orbitals. We denote the group of singles as  $f^{(1)}$ ,

which comprises a core hole and an electron; the group of doubles as  $f^{(2)}$ , which comprises an *additional* valence *e-h* pair; and so forth. The  $n$  in  $f^{(n)}$  can be understood as the order of excitations. *This enables a straightforward assignment of absorption features to excited states, making the interpretation of the spectrum simple.*

Third, an alternative solution for solving the MND model using DFT orbitals as input was introduced in Refs. [55–58], and good agreement has been achieved in some carbon systems and metals. In this method, a time-dependent matrix integral equation needs to be solved and matrix inversion is required for each point on the discretized time axis. Then a Fourier transformation is performed to obtain the spectrum. The determinant approach we proposed only requires a one-shot matrix inversion and no real-time evolution is involved. It is physically more intuitive and computationally less complex.

Finally, although many-electron configurations are employed for condensed-phase systems with hundreds to thousands of electrons in a supercell, the determinant calculation is *not at all intractable*. We have developed a heuristic search algorithm for finding the many-electron configurations that are important for determining the x-ray spectra [2]. For transition metal oxides (TMOs), it is found the x-ray absorption spectra (XAS) can be well defined by just  $10^5$  configurations up to the  $f^{(2)}$  order (not their superposition and no diagonalization of many-body Hamiltonian is needed), which are inexpensive calculations given the current computational capability.

It is, however, unknown yet how expensive the determinant calculations are in other systems apart from TMOs. It remains unclear if  $f^{(n)}$  configurations with  $n > 2$  are important for shaping the x-ray excitation spectra. Even with the heuristic search algorithm [2] that truncates the number of many-electron configurations, the number of meaningful  $f^{(n)}$  configurations still tends to diverge exponentially with respect to the shakeup order  $n$ . If one can estimate the spectral contributions from the  $f^{(n)}$  configurations before actually calculating them, it will be of great benefit for saving computational resources. In this work we propose a useful criterion for estimating the contributions of  $f^{(n)}$ , which helps one to decide at what  $n$  one should stop the determinant calculation. It is based on a singular-value decomposition (SVD) analysis of the  $\zeta$  matrix, the auxiliary matrix used to obtain the determinant transition amplitudes. An SVD analysis of the  $\zeta$  matrix reflects how the one-body basis set is rotated due to the perturbation of the core hole, and how the final-state occupied manifold is entangled with the initial state (typically the many-electron ground state). Besides TMOs, we have chosen several metallic systems such as Li and Cu metal and performed exhaustive calculations up to  $n = 5$  to test the convergence criterion in this work.

### B. Review of the determinant formalism

The central formula for calculating the x-ray absorption amplitudes from the ground-state (initial state)  $|\Psi_i\rangle$  to a specific final state  $|\Psi_f\rangle$  is [1,2]

$$\langle\Psi_f|O|\Psi_i\rangle = \sum_c (A_c^f)^* \langle\psi_c|o|\psi_h\rangle \quad (1)$$

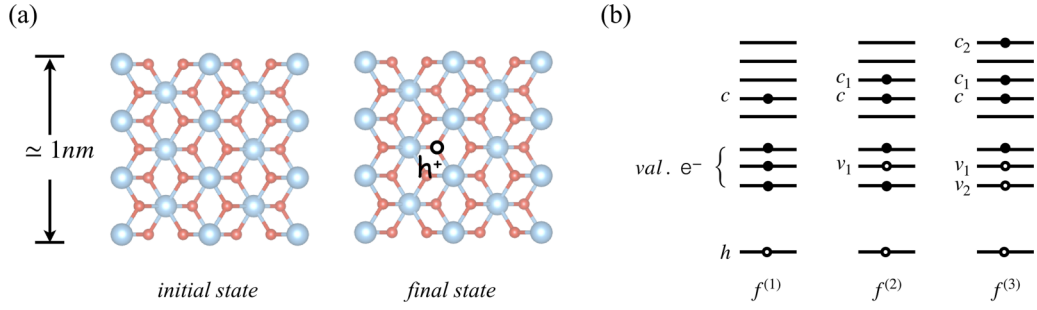


FIG. 1. (a) Graphical depicts of the x-ray initial-state and final-state system. Both of them are supercells. The final-state system contains an core hole ( $h^\dagger$ ) fixed to the excited atom, which is modeled by the corresponding core-hole pseudopotential. The supercell size should be larger than 1 nm so that the spurious interactions among core-hole images in periodic supercells are truncated. (b) Illustrations of x-ray excited states at different excitation order  $f^{(n)}$ , using a system with  $N = 3$  valence electrons and  $M = 8$  orbitals (core level excluded). Note that these free-fermion configurations are defined in the final-state picture, not the initial-state one.  $f^{(1)}$  configurations can be uniquely labeled by the orbital  $c$ ,  $f^{(2)}$  by three orbitals  $c$ ,  $c_1$ , and  $v_1$ , and  $f^{(3)}$  by five orbitals  $c$ ,  $c_1$ ,  $c_2$ ,  $v_1$ , and  $v_2$ .

in which the transition amplitude also takes a determinantal form

$$A_c^f = \det \begin{bmatrix} \xi_{f_1,1} & \xi_{f_1,2} & \cdots & \xi_{f_1,N} & \xi_{f_1,c} \\ \xi_{f_2,1} & \xi_{f_2,2} & \cdots & \xi_{f_2,N} & \xi_{f_2,c} \\ \vdots & \vdots & \ddots & \vdots & \vdots \\ \xi_{f_{N+1},1} & \xi_{f_{N+1},2} & \cdots & \xi_{f_{N+1},N} & \xi_{f_{N+1},c} \end{bmatrix} \quad (2)$$

and  $\xi_{ij} = \langle \psi_j | \tilde{\psi}_i \rangle$ , where  $|\tilde{\psi}_i\rangle$ 's are final-state orbitals,  $|\psi_j\rangle$ 's are initial-state orbitals, and  $N$  is the total number of valence electrons (excluding the core level) in the initial state. Therefore, the x-ray excited state has  $N + 1$  valence electrons due to excitation of the core level. An illustration of the initial and final state is shown in Fig. 1(a). In the calculation, both initial and final states are taken as supercells except that the core-excited atom in the final state is described using a modified pseudopotential. The perturbation from the core-excited atom leads to a rotation of orbital basis set from  $\{|\psi_j\rangle\}$  to  $\{|\tilde{\psi}_i\rangle\}$ .

Alternatively,  $A_c^f$  can be regarded as a single ‘‘Slater determinant’’ of a set of final-state orbitals ( $\tilde{\psi}_{f_1}, \tilde{\psi}_{f_2}, \dots, \tilde{\psi}_{f_{N+1}}$ ), expanded over the  $N + 1$  initial-state orbitals ( $\psi_1, \psi_2, \dots, \psi_N, \psi_c$ ) [rather than  $(\mathbf{r}_1, \mathbf{r}_2, \dots, \mathbf{r}_{N+1})$ ]. The first  $N$  of these orbitals are the lowest  $N$  occupied orbitals, and the last one  $\psi_c$  iterates over all the empty orbitals. The numerical evidence on the completeness of the initial-state basis set has been provided in previous work [2].

The first step we use to simplify the calculation is to move the summation over  $c$  into the determinant expression:

$$A^f \equiv \langle \Psi_i | O | \Psi_f \rangle = \det A^f, \quad A^f = \begin{bmatrix} \xi_{f_1,1} & \xi_{f_1,2} & \cdots & \xi_{f_1,N} & \sum_c \xi_{f_1,c} w_c^* \\ \xi_{f_2,1} & \xi_{f_2,2} & \cdots & \xi_{f_2,N} & \sum_c \xi_{f_2,c} w_c^* \\ \vdots & \vdots & \ddots & \vdots & \vdots \\ \xi_{f_{N+1},1} & \xi_{f_{N+1},2} & \cdots & \xi_{f_{N+1},N} & \sum_c \xi_{f_{N+1},c} w_c^* \end{bmatrix}. \quad (3)$$

There are an enormous number of combinations of  $(f_1, f_2, \dots, f_{N+1})$ , representing possible final-state configurations, but it is only meaningful to visit a small subset of this space. The determinant amplitude  $A^f$  is a significant number only when most of the indices  $(f_1, f_2, \dots, f_{N+1})$  of the

occupied orbitals overlap significantly with the lowest-energy configuration  $(1, 2, \dots, N + 1)$ , because in most realistic materials, the core hole is well screened and the orthogonality catastrophe does not occur. Therefore,  $(f_1, f_2, \dots, f_{N+1})$  may only differ from  $(1, 2, \dots, N + 1)$  by a few indices.

To simplify the notation, we may denote  $(f_1 = 1, f_2 = 2, \dots, f_N = N, f_{N+1} = c)$  as a single or  $f^{(1)}$  configuration,  $(f_1 = 1, f_2 = 2, \dots, f_{v_1-1} = v_1 - 1, f_{v_1} = v_1 + 1, \dots, f_{N-1} = N, f_N = c, f_{N+1} = c_1)$  as a double or  $f^{(2)}$  configuration, and so forth. The concepts of  $f^{(n)}$  are illustrated in Fig. 1(b).

There is a one-to-one correspondence between the excited states in the BSE and the  $f^{(1)}$  configuration in the determinant approach. In the core-level BSE, the excited states are labeled by the orbitals in the system with a core hole. Correspondingly, the  $f^{(1)}$  configurations in the determinant approach are also labeled by orbitals in the final-state system. However, the interaction between the electrons and the core hole are treated differently in the two approaches. In the BSE, screened Coulomb interactions obtained via random phase approximation, whereas in the determinant approach, electron-core-hole interactions are accounted for using exchange-correlation functionals of proper flavor.

Each line of  $A^f$  can be denoted as

$$a_i = \xi_{i,1} \cdots \xi_{i,N} \sum_c \xi_{i,c} w_c^*. \quad (4)$$

Next we can introduce the  $\zeta$  matrix to calculate all the  $A^f$ 's in an iterative manner. The  $\zeta$  matrix is the linear transformation from  $a_i$ 's of the occupied orbitals ( $i \leq N$  plus  $a_{N+1}$ ) to the  $a_i$ 's of the empty orbitals ( $i > N$ )

$$\begin{bmatrix} a_{N+1} \\ a_{N+2} \\ \vdots \\ a_M \end{bmatrix} = \begin{bmatrix} 0 & 0 & \cdots & 1 \\ \zeta_{N+2,1} & \zeta_{N+2,2} & \cdots & \zeta_{N+2,N+1} \\ \vdots & \vdots & \ddots & \vdots \\ \zeta_{M,1} & \zeta_{M,2} & \cdots & \zeta_{M,N+1} \end{bmatrix} \begin{bmatrix} a_1 \\ a_2 \\ \vdots \\ a_{N+1} \end{bmatrix}. \quad (5)$$

Rewriting the above matrix multiplication in a compact form, we have  $A^{\text{new}} = \zeta A^{\text{ref}}$ , where  $(\zeta)_{ij} = \zeta_{N+i,j}$ . Thus the  $\zeta$  matrix can be obtained from  $\zeta = A^{\text{new}} (A^{\text{ref}})^{-1}$ .

With the auxiliary  $\zeta$  matrix, we can quickly calculate the determinants for many excited-state configurations without repeatedly using the  $O(N^3)$  determinant algorithm. Instead, an  $O(1)$  algorithm can be used. Once the determinant for the ground state  $A^{\text{ref}}$  is obtained, the determinant of each excited state can be computed by multiplying  $A^{\text{ref}}$  by a prefactor. The prefactor is a small determinant composed of the matrix elements of the  $\zeta$  matrix. For example, the amplitude of a single ( $f^{(1)}$ ), double ( $f^{(2)}$ ), and triple ( $f^{(3)}$ ) configuration can be obtained respectively as

$$A^c = \zeta_{c,N} A^{\text{ref}}, \quad A^{c;c_1,v_1} = \det \begin{bmatrix} \zeta_{c,v_1} & \zeta_{c,N} \\ \zeta_{c_1,v_1} & \zeta_{c_1,N} \end{bmatrix} A^{\text{ref}},$$

$$A^{c;c_1,v_1;c_2,v_2} = \det \begin{bmatrix} \zeta_{c,v_2} & \zeta_{c,v_1} & \zeta_{c,N} \\ \zeta_{c_1,v_2} & \zeta_{c_1,v_1} & \zeta_{c_1,N} \\ \zeta_{c_2,v_2} & \zeta_{c_2,v_1} & \zeta_{c_2,N} \end{bmatrix} A^{\text{ref}}. \quad (6)$$

These are the essential formulas to obtain the amplitudes for the excited-state configuration with the  $O(1)$  updating algorithm. A  $f^{(n)}$  configuration corresponds to a  $n \times n$  sub-determinant of the  $\zeta$  matrix.

Directly enumerating all such subdeterminants is a computationally expensive task. Also, it may not be necessary to do so because the  $\zeta$  matrix could be a sparse matrix. In previous work [2] we have proposed a heuristic search algorithm for quickly finding significant subdeterminants of a sparse matrix. Our general search algorithm is not merely specific to the  $\zeta$  matrix for x-ray spectroscopic problems.

What was overlooked in the previous work, however, is that the  $\zeta$  matrix for x-ray excitations does have structures. It can be seen that the  $\zeta$  matrices for  $\text{SiO}_2$ ,  $\text{TiO}_2$ ,  $\text{CrO}_2$  all display a vertical (horizontal) stripe pattern (Fig. 8(d) of Ref. [2]). This stripe pattern can also be seen in other chosen examples, which are discussed later in this work. These stripe patterns imply a further simplification of the  $\zeta$  matrix that it can be approximately expressed as the Kronecker product of two vectors:

$$\zeta_{ij} \sim a_i b_j. \quad (7)$$

If  $\zeta_{ij} \sim a_i b_j$  strictly holds, then all the  $n \times n$  subdeterminants for  $n > 1$  will be exactly zero and only the  $f^{(1)}$  amplitudes are nonvanishing. It is the deviation of  $\zeta_{ij}$  from  $a_i b_j$  that determines the size of higher-order terms  $f^{(n)}$  ( $n > 1$ ). If one can expand  $\zeta_{ij}$  into just a few terms, then it is highly probable that the size of higher-order terms can be quickly estimated. In this regard, a singular-value decomposition (SVD) of the  $\zeta$  matrix is most relevant for this problem. SVD has been widely used to analyze the entanglement structure between two quantum many-body systems [60–62].

In the following discussion, we first provide and prove two theorems that will give upper bounds on the size of the  $f^{(n)}$  terms, for a specific  $n$ , using SVD analysis for the  $\zeta$  matrix. The bounds will enable one to determine the contribution of the  $f^{(n)}$  terms to the x-ray excitation spectrum, without explicitly calculating these terms. This will save a substantial amount of computational cost and help one obtain a meaningful x-ray excitation spectrum faster. Then we apply the theorems to several small band-gap and metallic systems, in which higher-order terms  $f^{(n)}$  ( $n > 1$ ) are expected to contribute to the spectrum significantly. It is, however, found

that in *none* of the chosen systems, the contribution from  $f^{(n)}$  ( $n > 2$ ) can significantly alter the spectral line shapes (more precisely, the peak intensity ratios). In other words, the spectra have already taken shape at the order of  $n = 2$ .

## II. RESULTS AND DISCUSSION

### A. Two theorems about subdeterminants

*Theorem 1.* Let  $D$  be the determinant of an  $n \times n$  submatrix that spans over rows  $i_1, i_2, \dots, i_n$  and columns  $j_1, j_2, \dots, j_n$  of an  $N \times M$  matrix  $\zeta$ . Suppose the singular-value decomposition (SVD) of  $\zeta$  is

$$\zeta_{ij} = \sum_k s^k a_i^k b_j^k, \quad (8)$$

where  $\{s^k\}$  are the singular values of  $\zeta$ , and  $a_i^k$  ( $b_j^k$ ) is a normalized vector for a given  $k$ . Then the determinant  $D$  can be expanded as the summation

$$D = \sum_{k_1 < k_2 < \dots < k_n} s^{k_1} s^{k_2} \dots s^{k_n} D_{[k_\mu]}^a D_{[k_\mu]}^b \quad (9)$$

in which  $D_{[k_\mu]}^a$  ( $D_{[k_\mu]}^b$ ) is the determinant of the submatrix that spans over rows  $i_1, i_2, \dots, i_n$  and columns  $k_1, k_2, \dots, k_n$  of the matrix  $a_i^k$  ( $b_j^k$ ).

*Proof.* Without loss of generality, we may assume  $i_1 = j_1 = 1, i_2 = j_2 = 2, \dots, i_n = j_n = n$ . According to the definition of the determinant,  $D$  can be expanded using the Levi-Civita symbol:

$$D = \sum_{l_1 l_2 \dots l_n = 1}^n \varepsilon_{l_1 l_2 \dots l_n} \zeta_{1 l_1} \zeta_{2 l_2} \dots \zeta_{n l_n}. \quad (10)$$

Inserting the SVD expression of the matrix element  $\zeta_{ij}$  as in Eq. (8) (examples of  $\zeta$  can be found in Fig. 3),

$$\begin{aligned} D &= \sum_{l_1 l_2 \dots l_n = 1}^n \varepsilon_{l_1 l_2 \dots l_n} \left( \sum_{k_1} s^{k_1} a_1^{k_1} b_{l_1}^{k_1} \right) \dots \left( \sum_{k_n} s^{k_n} a_n^{k_n} b_{l_n}^{k_n} \right) \\ &= \sum_{l_1 l_2 \dots l_n = 1}^n \varepsilon_{l_1 l_2 \dots l_n} \left[ \sum_{k_1 k_2 \dots k_n} s^{k_1} s^{k_2} \dots s^{k_n} a_1^{k_1} b_{l_1}^{k_1} \dots a_n^{k_n} b_{l_n}^{k_n} \right] \\ &= \sum_{k_1 k_2 \dots k_n} s^{k_1} s^{k_2} \dots s^{k_n} a_1^{k_1} \dots a_n^{k_n} \left[ \sum_{l_1 l_2 \dots l_n = 1}^n \varepsilon_{l_1 l_2 \dots l_n} b_{l_1}^{k_1} \dots b_{l_n}^{k_n} \right]. \end{aligned} \quad (11)$$

Note that the inner summation with respect to  $l_\nu$  for a specific  $\{k_\mu\}$  ( $\mu, \nu = 1, 2, \dots, n$ ) gives rise to a determinant, which can be denoted as

$$D_{[k_\mu]}^b \equiv \sum_{l_1 l_2 \dots l_n = 1}^n \varepsilon_{l_1 l_2 \dots l_n} b_{l_1}^{k_1} \dots b_{l_n}^{k_n}. \quad (12)$$

This determinant corresponds to the submatrix  $b_l^k$  formed by row  $1, 2, \dots, n$  and column  $k_1, k_2, \dots, k_n$ .

In the outer summation of Eq. (11), each index  $k_\mu$  can range from 1 to the number of singular values.  $D_{[k_\mu]}^b$  is nonzero only when  $k_1, k_2, \dots, k_n$  are not equal to each other, thus placing constraints on values of  $k_\mu$  in the outer summation.

Next, we may consider the case where the  $n$  values of  $k_\mu$  are taken from  $1, 2, \dots, n$ , without loss of generality. Note that there is no ordering presumed in the outer summation of  $k_\mu$ , therefore summing over all  $k_\mu$ 's will generate  $n!$  permutations of  $1, 2, \dots, n$ . For these  $n!$  permutations, the corresponding  $D_{[k_\mu]}^b$  will have the same absolute value, and its  $\pm$  sign depends on whether the permutation is odd or even, due to the nature of determinant. If we enforce ordering  $k_1 < k_2 < \dots < k_n$ , we may use the Levi-Civita symbol to represent the sign due to permutation:

$$D = \sum_{k_1 k_2 \dots k_n} s^{k_1} s^{k_2} \dots s^{k_n} a_1^{k_1} \dots a_n^{k_n} D_{[k_\mu]}^b$$

$$= \sum_{k_1 < k_2 < \dots < k_n} s^{k_1} s^{k_2} \dots s^{k_n} \sum_{l_1 l_2 \dots l_n} a_1^{l_1} \dots a_n^{l_n} \varepsilon_{l_1 l_2 \dots l_n} D_{[k_\mu]}^b, \quad (13)$$

where the tuple  $l_1 l_2 \dots l_n$  iterate over all permutation of  $k_1 < k_2 < \dots < k_n$ . Therefore,

$$D = \sum_{k_1 < k_2 < \dots < k_n} s^{k_1} s^{k_2} \dots s^{k_n} D_{[k_\mu]}^a D_{[k_\mu]}^b. \quad (14)$$

**Theorem 2.** The absolute value of the determinant of an  $n \times n$  submatrix of  $\zeta$  is bound by the product of its largest  $n$  singular values provided by SVD

$$|D^{n \times n}| \leq \sum_{k_1 < k_2 < \dots < k_n} s^{k_1} s^{k_2} \dots s^{k_n}, \quad (15)$$

where the singular values satisfy  $s^1 \geq s^2 \geq \dots \geq s^n > 0$ .

*Proof.* We may start by proving the absolute value of the determinant  $D_{[k_\mu]}^a$  ( $D_{[k_\mu]}^b$ ) is bound by 1. Without loss of generality, we may again assume  $i_1 = 1, i_2 = 2, \dots, i_n = n$  and  $k_1 = 1, k_2 = 2, \dots, k_n = n$ . According to its definition:

$$D_{[k_\mu]}^a = \begin{vmatrix} a_1^1 & a_1^2 & \dots & a_1^n \\ a_2^1 & a_2^2 & \dots & a_2^n \\ \vdots & \vdots & \ddots & \vdots \\ a_n^1 & a_n^2 & \dots & a_n^n \end{vmatrix}. \quad (16)$$

Each row of the above determinant is a vector  $\mathbf{a}_{1 \times n}^k = (a_1^k, a_2^k, \dots, a_n^k)$ , which is a truncation of a full  $1 \times N$  vector  $\mathbf{a}^k = (a_1^k, a_2^k, \dots, a_N^k)$ .  $N$  is the first dimension of  $\zeta$  and  $n \leq N$ . Since the matrix  $a_i^k$  is obtained from SVD of  $\zeta$ , each of its row vector is normalized to 1:  $|\mathbf{a}^k| = 1$ , and therefore:

$$|\mathbf{a}_{1 \times n}^k| \leq 1. \quad (17)$$

The geometric meaning of the determinant  $D_{[k_\mu]}^a$  is the volume of a parallelepiped spanned by  $n$  vectors  $\mathbf{a}^k$ , where  $k = 1, 2, \dots, n$ . Since the length of each of its edge  $|\mathbf{a}_{1 \times n}^k| \leq 1$ , then the volume of the parallelepiped will be no larger than 1, and thus  $|D_{[k_\mu]}^a| \leq 1$  ( $|D_{[k_\mu]}^b| \leq 1$ ).

Using the conclusion of theorem 1,

$$|D^{n \times n}| \leq \sum_{k_1 < k_2 < \dots < k_n} |s^{k_1} s^{k_2} \dots s^{k_n} D_{[k_\mu]}^a D_{[k_\mu]}^b|$$

$$\leq \sum_{k_1 < k_2 < \dots < k_n} s^{k_1} s^{k_2} \dots s^{k_n}. \quad (18)$$

Note that all the singular values of  $\zeta$  are non-negative.

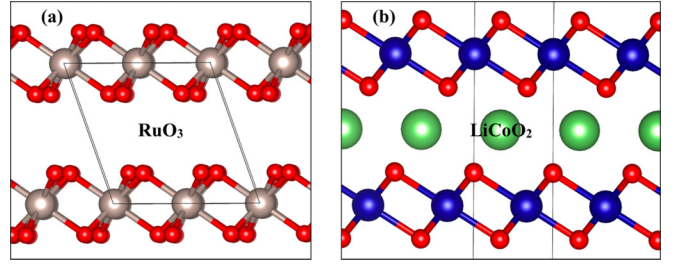


FIG. 2. Layered structures (side view) of  $\text{RuO}_3$  (a) and  $\text{LiCoO}_2$  (b). The unit cells are outlined by the thin black lines.

## B. An analysis of $\zeta$ matrices with singular-value decomposition

We analyze several representative examples here to illustrate the usefulness of the two theorems for  $\zeta$  matrices: A 1D single-atom chain at half-filling, the C  $K$  edge of graphite, the Cu  $K$  edge of copper, the Li  $K$  edge of lithium metal, and the O  $K$  edge of rutile  $\text{TiO}_2$ ,  $\text{CrO}_2$ ,  $\text{RuO}_3$ , and  $\text{LiCoO}_2$ . The crystal structures of  $\text{RuO}_3$ , and  $\text{LiCoO}_2$  are shown in Fig. 2. Both systems are layered structures that will allow lithium insertion/removal, and are being studied as cathode prototypes of rechargeable batteries. The chosen systems are gapless except for  $\text{TiO}_2$  and  $\text{LiCoO}_2$ , which have a DFT-PBE band gap of 2.1 and 1.8 eV (with a Hubbard  $U$  value of 3.3 eV on the Co atom), respectively.

The tight-binding model for the 1D chain reads

$$H = -t \sum_{j=1}^N (c_{j+1}^\dagger c_j + c_j^\dagger c_{j+1}), \quad (19)$$

where a periodic boundary condition is employed and each site has double occupancy. The above model is considered as the initial-state Hamiltonian  $H_i$ . The core-hole potential is assumed to act on a single site (the site at  $j = 0$ ):  $V_c = \Delta V c_0^\dagger c_0$ , thus the final-state Hamiltonian is  $H_f = H_i + V_c$ . It can be solved that the  $1p$  wave functions for  $H_i$  are

$$|k\sigma\rangle = \frac{1}{\sqrt{N}} \sum_{j=0}^N e^{ikj} |j\sigma\rangle, \quad (20)$$

where  $k = 0, \frac{1}{N}, \dots, \frac{N-1}{N}$  and  $\sigma = \uparrow, \downarrow$ . We can define the  $1p$  XAS matrix element as

$$\langle k\sigma | j = 0, \sigma \rangle = \frac{1}{\sqrt{N}}, \quad (21)$$

which serves to mimic  $\langle \psi_c | o | \psi_h \rangle$  as in Eq. (1). Because we have not introduced any actual real-space orbital in the 1D tight-binding model, we use the projection onto the excited site as the  $1p$  transition amplitude.

In the actual calculation, we choose the number of sites  $N = 200$ , the number of electrons  $N_e = 200$  (half-filled),  $t = 1$ , a perturbation potential of  $\Delta V = -100$  at the excited site to simulate the core hole effect (set to 100 for exaggeration). We find the determinant spectrum barely changes after  $\Delta V < -100$ .

First, we plot the  $\zeta$  matrices for the XAS (Li, C, O, and Cu  $K$  edges) of six chosen systems in order to exemplify the

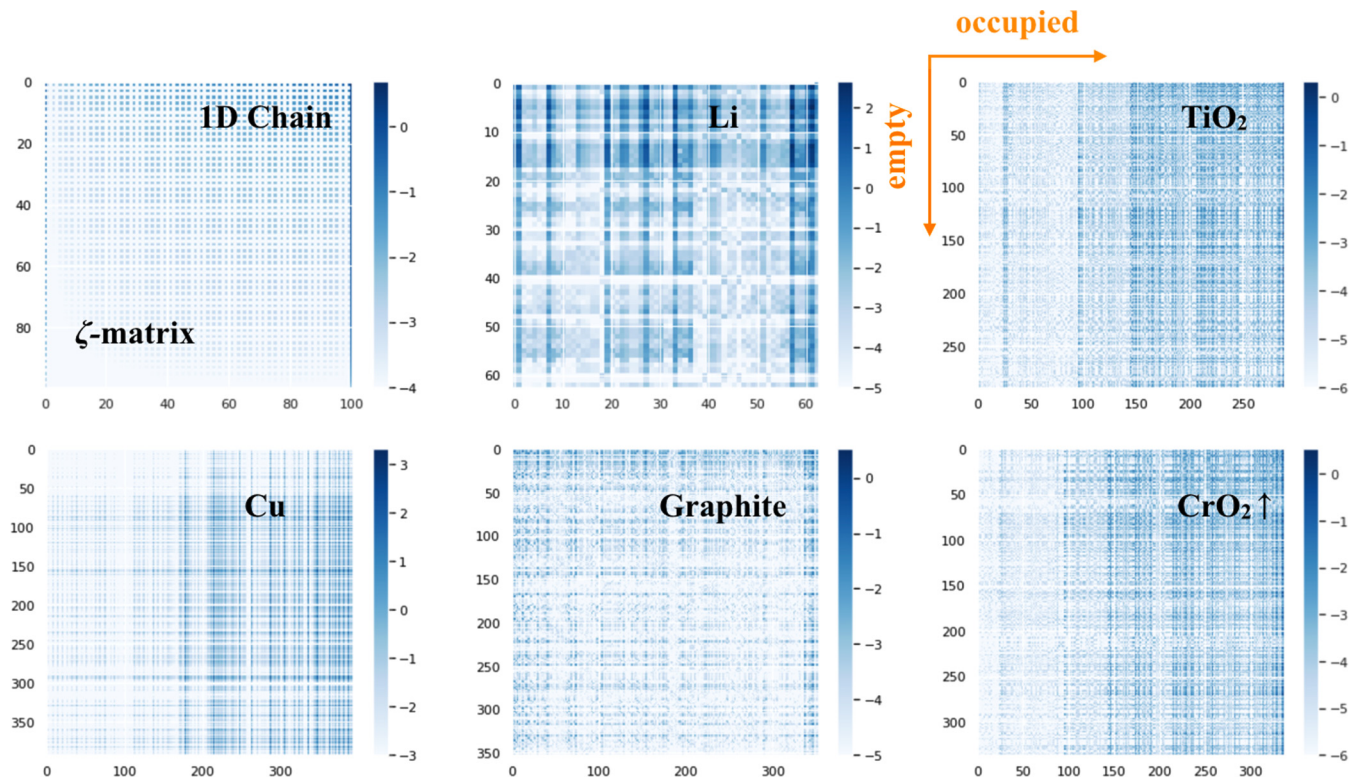


FIG. 3. Heat-map plot of  $\log_{10} |\zeta_{ij}|$  of the XAS  $\zeta$  matrices of several chosen systems for illustrating the cross-stripe pattern. If not plotted in logarithm scale, the  $\zeta$  matrices will appear to be sparse. The rows correspond to empty orbitals and the columns to occupied orbitals. The number of occupied orbitals in the 1D chain, Li, TiO<sub>2</sub>, Cu, graphite, and CrO<sub>2</sub> (the spin-up channel) supercell are 100, 64, 288, 352, 392, and 336, respectively, which determines the number of columns.

aforementioned stripe pattern. Once we have completed the  $\Delta$ SCF calculation for both the initial and final state, the  $\zeta$  matrices can be calculated using Eq. (5). Several  $\zeta$  matrices are shown in Fig. 3. Although the chosen systems are vastly different in terms of crystal symmetry and bonding nature, it can be seen that all the plotted  $\zeta$  matrices display a cross-stripe pattern that runs both vertically and horizontally. This cross-stripe pattern suggests that the  $\zeta$  matrix for x-ray excitations can be universally expressed in terms of the Kronecker product of two vectors:  $\zeta_{ij} \sim a_i b_j$ , with a few small residual terms. Thus it becomes natural to introduce an SVD analysis to the  $\zeta$  matrix, and apply the two theorems proved above to determine the spectral convergence with respect to shakeup order.

The 20 most significant singular values of the  $\zeta$  matrices of the chosen systems are shown in Fig. 4 (the singular values are plotted logarithmically). The first five largest singular values (denoted as  $s^i$ ) are also tabulated in Table I. It can immediately be seen for all the  $\zeta$  matrices that only a few singular values are larger than 1, especially for graphite, TiO<sub>2</sub>, LiCoO<sub>2</sub>, and the insulating (spin-down) channel of CrO<sub>2</sub> with only one  $s^i > 1.0$ . The latter three are systems with a large band gap. The other systems only have two singular values larger than 1. Note that in Li,  $s^3 = 0.977$  and  $s^4 = 0.653$ , which can be rounded to 1. In all the cases,  $s^i < 0.1$  for  $i > 10$ , which are orders of magnitude smaller than  $s^1$ . This means only a few singular values  $s^i$  are relevant for the analysis of shakeup orders.

With these numerical results and the properties of  $\{s^i\}$ , we can revisit the two theorems and discuss the contributions

from different shakeup order  $f^{(n)}$  to the x-ray spectra. Because the vast majority of  $s^i$  are small, we could take the product of the leading  $s^i$  to form an analysis of order of approximation. As indicated in Theorem 1, the  $n \times n$  subdeterminants corresponding to the  $f^{(n)}$  terms are associated with the coefficients  $s^{k_1} s^{k_2} \dots s^{k_n}$ . We may thus take the largest  $n$  singular values  $s^1$  and calculate their product to estimate the contribution of  $f^{(n)}$ :

$$f^{(1)} : s^1 \quad f^{(2)} : s^1 s^2 \quad f^{(3)} : s^1 s^2 s^3 \dots \quad (22)$$

The cumulative product  $s^1 s^2 \dots s^n$  of some leading-order singular values are also shown in Table I. For Li, RuO<sub>3</sub>, Cu, CrO<sub>2</sub>  $\uparrow$ ,  $s^1 s^2$  is significantly larger than  $s^1$  because  $s^2 > 1.5$ . This suggests the contribution of the  $f^{(2)}$  terms is of the same order of magnitude of  $f^{(1)}$ . An extreme case is Li in which even  $s^1 s^2 s^3 s^4 \approx 591$  is larger than  $s^1 \approx 479$ . This requires one to go beyond  $f^{(1)}$  in the XAS determinant calculation for these systems.

### C. XAS calculated by the determinant formalism

To test how good this empirical estimate is, we perform determinant calculations for XAS of the chosen systems, at least at the order of  $f^{(2)}$ . The obtained spectra decomposed by different shakeup orders are shown in Fig. 5 (odd rows). We find it is indeed true that the contribution from the  $f^{(2)}$  terms is as significant as  $f^{(1)}$  in Li, RuO<sub>3</sub>, Cu, CrO<sub>2</sub>  $\uparrow$  (as studied in Refs. [1,2]). In every case, the contribution from  $f^{(2)}$  constitutes more than 40% of the entire computed spectrum. In particular for Li, a trend of convergence is only

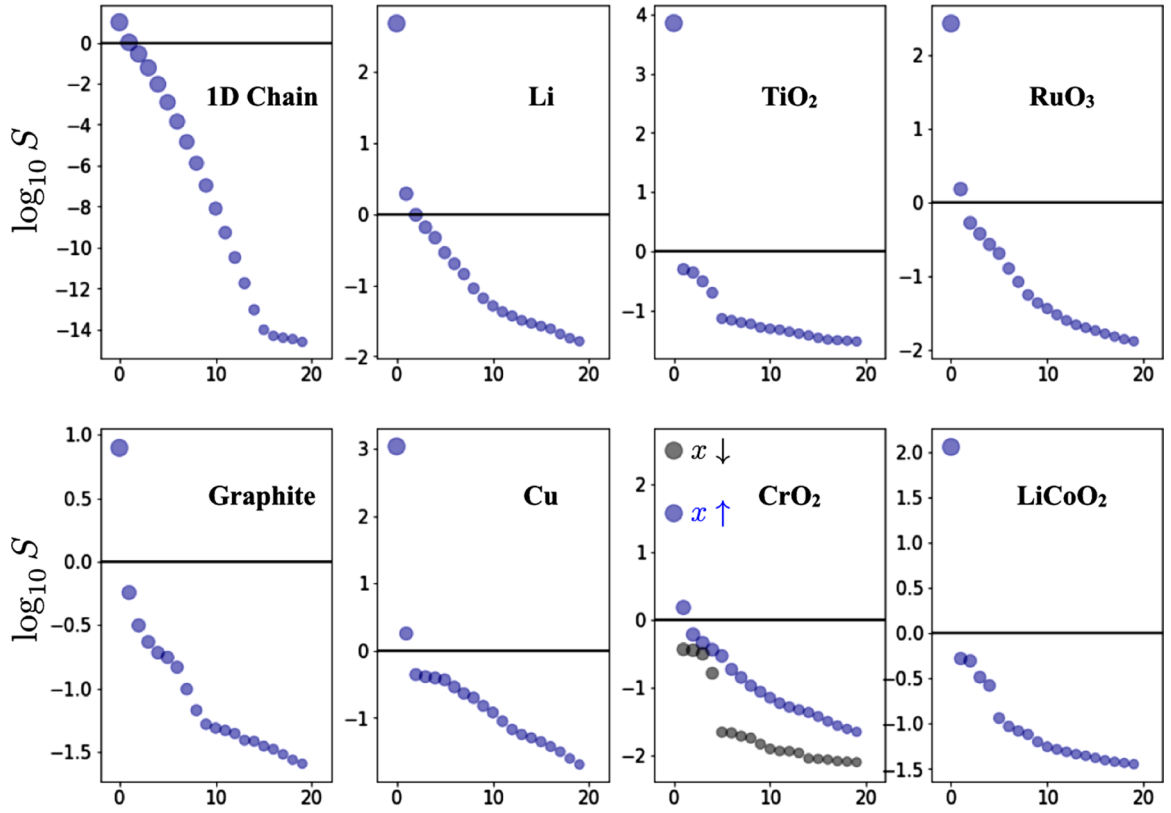


FIG. 4. 20 most significant singular values of the  $\zeta$  matrices. The singular values are positive definite and scaled logarithmically. The horizontal line at  $S = 1$  is used to divide values larger than 1 and smaller than 1. For  $\text{CrO}_2$ , two series of singular values for spin-wise  $\zeta$  matrices are plotted.

seen after including the  $f^{(4)}$  terms. The contributions from  $f^{(1)}$ ,  $f^{(2)}$ ,  $f^{(3)}$ ,  $f^{(4)}$ , and  $f^{(5)}$  to the full spectrum ( $f^{(1)} + f^{(2)} + f^{(3)} + f^{(4)} + f^{(5)}$ ) are 29.7%, 51.3%, 14.8%, 3.7%, and 0.5%. This is consistent with the fact that  $s^1 s^2 \approx 927$ ,  $s^1 s^2 s^3 \approx 906$ , and  $s^1 s^2 s^3 s^4 \approx 591$  are comparable to  $s^1 \approx 479$  in this system. But note that the contribution  $f^{(n)}$  is not entirely proportional to the cumulative product  $s^1 s^2 \dots s^n$ . It is observed that  $f^{(n)}$  decays more quickly than  $s^1 s^2 \dots s^n$  as  $n$  increases. This is because we have not taken into account the decomposed determinants  $D_{[k_\mu]}^a$  and  $D_{[k_\mu]}^b$  in this empirical estimate, and  $|D_{[k_\mu]}^a|, |D_{[k_\mu]}^b| < 1$  holds strictly as proved in Theorem 2.

In other investigated systems such as graphite,  $\text{LiCoO}_2$ ,  $\text{TiO}_2$ , and  $\text{CrO}_2\downarrow$ , the contribution from the  $f^{(2)}$  terms is

noticeably less significant, constituting less than 30% of the full spectrum. Their corresponding second largest singular values  $s^2 < 0.6$ , suggesting that  $s^1 s^2 < s^1$  and hence  $f^{(2)}$  would not be as important as the  $f^{(1)}$  terms. One severe deviation from this estimate would be the tight-binding 1D chain. The corresponding  $s^1 s^2 \approx 10.25$ , which is comparable to  $s^1 \approx 9.97$ . However, the  $f^{(2)}$  contribution is tiny, about 6.1% of the full ( $f^{(1)} + f^{(2)}$ ) spectrum. Again, this is because the decomposed determinants  $D_{[k_\mu]}^a$  and  $D_{[k_\mu]}^b$  are missing. In this regard, it would be better to view the cumulative product  $s^1 s^2 \dots s^n$  as the *upper bound* of the  $f^{(n)}$  contribution. In other words, if  $s^1 s^2 \dots s^n$  is significantly small compared to the leading order terms ( $s^1$  and  $s^1 s^2$ ), then it is already safe to neglect the  $f^{(n)}$  terms.

TABLE I. The largest five singular values of the zeta matrices of the studies systems, and their cumulative products.

System	$s^1$	$s^2$	$s^3$	$s^4$	$s^5$	$s^1 s^2$	$s^1 s^2 s^3$	$s^1 s^2 s^3 s^4$	$s^1 s^2 s^3 s^4 s^5$	
1D chain	9.9683	1.0287	0.2810	0.0592	0.0094	10.2545	2.8820	0.1707	0.0016	$\eta_3 = 0.28$
Li	478.8850	1.9354	0.9774	0.6528	0.4657	926.8103	905.8236	591.2829	275.3625	$\eta_5 = 0.30$
$\text{TiO}_2$	7092.6499	0.5008	0.4417	0.3118	0.2006	3552.0365	1569.0875	489.1961	98.1572	$\eta_3 = 0.22$
$\text{RuO}_3$	267.8267	1.5267	0.5323	0.3790	0.2721	408.8852	217.6645	82.4916	22.4428	$\eta_4 = 0.21$
Graphite	7.8617	0.5691	0.3137	0.2325	0.1913	4.4744	1.4035	0.3264	0.0624	$\eta_3 = 0.18$
Cu	1076.8833	1.7903	0.4386	0.4087	0.3919	1927.8910	845.5359	345.5765	135.4185	$\eta_3 = 0.44$
$\text{CrO}_2 \uparrow$	37.0903	1.5178	0.6071	0.4586	0.3631	56.2962	34.1768	15.6735	5.6917	$\eta_4 = 0.28$
$\text{CrO}_2 \downarrow$	310.3019	0.3667	0.3556	0.3157	0.1634	113.7812	40.4625	12.7736	2.0867	$\eta_2 = 0.37$
$\text{LiCoO}_2$	113.3031	0.5227	0.4932	0.3257	0.2632	59.2231	29.2065	9.5120	2.5036	$\eta_3 = 0.26$

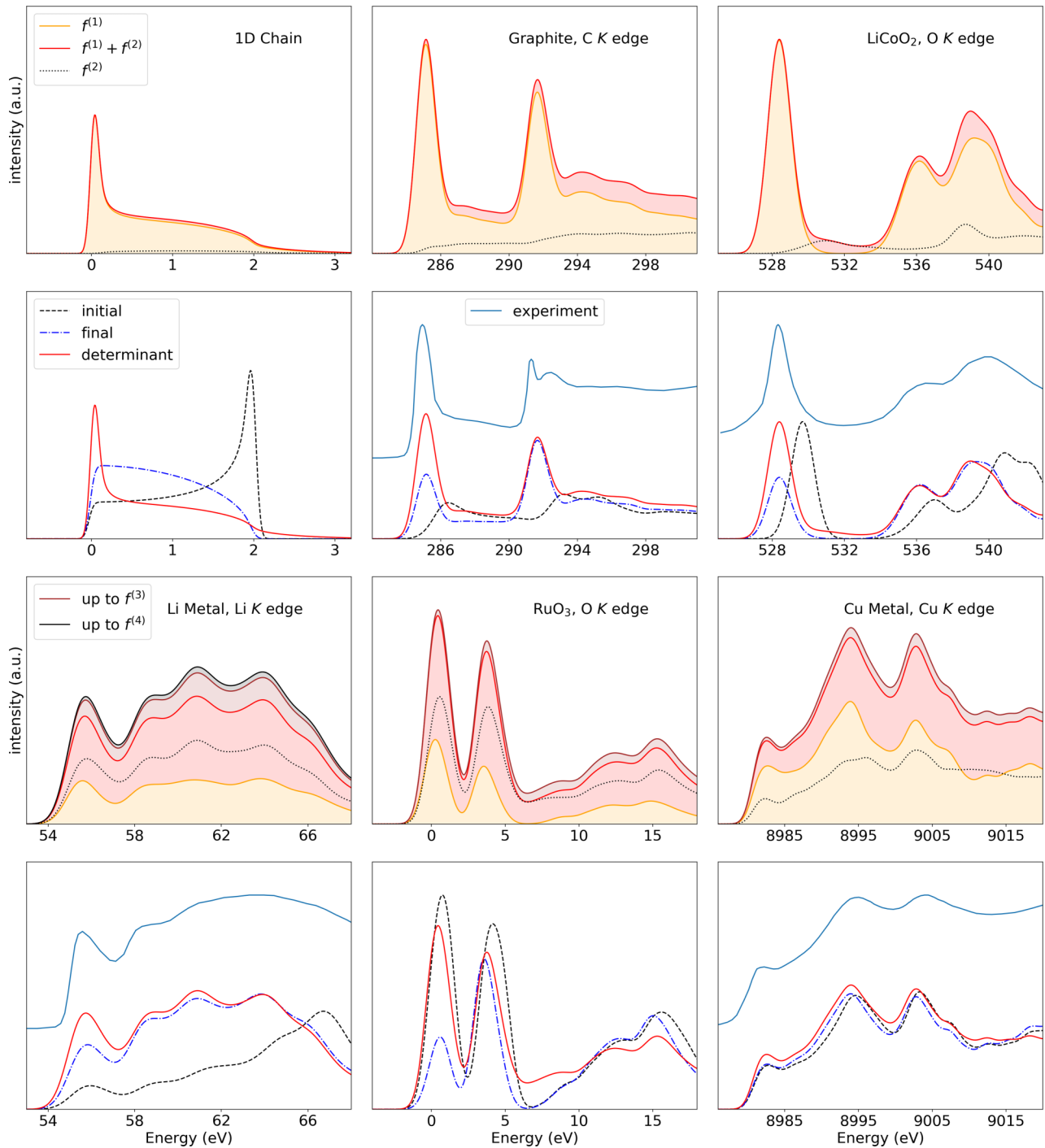


FIG. 5. Odd rows: Comparison of the determinant spectra at different shakeup orders. Even rows: Comparison of the determinant spectra, with the initial- and final-state spectra, and with available experimental spectra. A high-order determinant spectrum is not plotted if it appears to overlap on the determinant spectrum at one lower order (for example, the Li spectrum up to  $f^{(5)}$  appear to overlap with the one up to  $f^{(4)}$ ). The determinant spectra are scaled for comparing to the initial- and final-state spectra, according to the absorption peak at around 293 eV for graphite, 536 eV for LiCoO<sub>2</sub>, 64 eV for Li, 4 eV for RuO<sub>3</sub>, and 9005 eV for Cu, respectively. The experimental spectra are digitized from Ref. [63] (graphite), [64] (LiCoO<sub>2</sub>), [65] (Li), and [66] (Cu). The double-peak structure of the  $\sigma^*$  peak near 292.5 eV in graphite could be due to lattice vibrational effects, according to a recent work [59].

To define the smallness of the cumulative product, we may introduce the ratio  $\eta_n$  such that:  $\eta_n \max\{s^1 s^2 \cdots s^m\} = s^1 s^2 \cdots s^n$ , where  $\max\{s^1 s^2 \cdots s^m\}$  is the maximum of the cumulative product. According to

the examples studied in this work, we find one could safely neglect the  $f^{(n)}$  configurations with  $\eta_n < 0.5$ .

Although we have gone beyond  $f^{(2)}$  configurations in the determinant calculation, we still find the spectra for all the



cases studied in this work can be well defined by just the configurations up to  $f^{(2)}$ . This applies even to Li, in which up to  $f^{(5)}$  configurations are included. The  $f^{(2)}$  configurations slightly increase intensities of the two absorption humps at 61 and 64 eV compared to the absorption peak at 56 eV. And the spectra beyond  $f^{(2)}$  (summed from  $f^{(1)}$  to  $f^{(n)}$  for  $n = 3, 4, 5$ ) can basically be reproduced by scaling up the  $f^{(1)} + f^{(2)}$  spectrum using an energy-independent factor.

Here we take a closer examination of the intensity contribution from  $f^{(2)}$  configurations (as shown by black dotted curves in Fig. 5). The  $f^{(2)}$  contributions in the 1D chain, graphite, and LiCoO<sub>2</sub> (the first row of Fig. 5) are different from the ones as in Li, RuO<sub>3</sub>, and Cu (the third row of Fig. 5). In the former group, the  $f^{(2)}$  contribution does not have as many absorption features compared to  $f^{(1)}$ . In particular, the  $f^{(2)}$  contribution does not have a well-defined peak at the absorption edge as manifests in  $f^{(1)}$ . In the latter group, the  $f^{(2)}$  contribution mimics the  $f^{(1)}$  contribution in that they have similar absorption structures (peaks). All the absorption peaks that appear in  $f^{(1)}$  also appear in  $f^{(2)}$ , including the peaks at the absorption onset. A primary reason for the  $f^{(2)}$  contribution mimicking the  $f^{(1)}$  one in Li, RuO<sub>3</sub>, and Cu is due to low-energy  $e$ - $h$  pair production in these metallic systems. There are many orbitals of similar energies near the Fermi level in the final-state system (the supercell that contains an impurity for modeling core-excited states). More specifically, there are more than 12 orbitals within an energy window of 0.3 eV at the  $\Gamma$  point of the supercell, as found by the  $\Delta$ SCF calculations. Some of these orbitals are occupied and some are not. The majority of the  $f^{(2)}$  configurations in these systems can be understood as a transition from the core level to one empty final-state orbital  $c$ , coupled with a low-energy  $e$ - $h$  pair (as labeled by  $c_1$  and  $v_1$ ), whose excitation energy is negligibly small. Therefore the spectral contribution from  $f^{(2)}$  mimics the one from  $f^{(1)}$ , which is only defined by empty final-state orbitals, in a one-body manner. *This partially explains why the one-body final-state method can often reproduce the XAS of many metallic systems adequately, even though the physics of MND theory is completely missing.*

The  $f^{(2)}$  contributions in the 1D chain, graphite, and LiCoO<sub>2</sub> are more complex to analyze, which involves not just low-energy  $e$ - $h$  pairs near the Fermi level/band gap. In graphite, for instance, many  $f^{(2)}$  configurations that contribute modestly to XAS are composed of a core-level transition to  $c$  which is coupled to an  $e$ - $h$  pair with  $c_1$  being a low-lying empty orbital ( $\pi^*$ ), and  $v_1$  going over the continuum of occupied orbitals that span more than 8 eV ( $\pi$  and  $\sigma$  continuum). So the transition energy should be added from the two  $e$ - $h$  pairs:  $E = (\varepsilon_c - \varepsilon_h) + (\varepsilon_{c_1} - \varepsilon_{v_1})$ , in which both  $\varepsilon_c - \varepsilon_h$  and  $\varepsilon_{c_1} - \varepsilon_{v_1}$  can vary across a wide energy range. This explains why the  $f^{(2)}$  spectral contribution in graphite is smeared out without well-defined peaks. Similar analysis applies to the  $f^{(2)}$  continuum between 530 and 534 eV in LiCoO<sub>2</sub>, which involves transitions from the core level and some valence orbitals  $v_1$  (mainly O  $2p$ ) around 4 eV below the valence band maximum (VBM) to two low-lying empty orbitals  $c$  and  $c_1$ . This  $f^{(2)}$  continuum fills out the energy gap between 530 and 534 eV, and explains why there is no spectral gap between near-edge peaks (<6 eV from onset) and the high-energy humps (>6 eV from onset) in the O  $K$  edge

of TMOs, although there is no single-body orbital within this gap. Such is true for the energy gap near 6 eV in RuO<sub>3</sub>.

It should be noted that configuration interaction is absent from the above analysis of  $f^{(2)}$  configurations. Interaction within  $f^{(2)}$  may introduce excitonic effects between  $c_1$  and  $v_1$  and plasmon excitations. So far there is no electron-plasmon (plasmaron) coupling present in the determinant approach. Configuration interaction between  $f^{(1)}$  and  $f^{(2)}$  may remix the spectral contribution from the two sets of configurations and modify the shakeup effects. So far the ratio of the intensities of the near-edge peaks to the high-energy humps in TMOs is still too high in the determinant calculation up to  $f^{(2)}$ , as compared with experiments. Introducing configuration interaction may resolve this problem, which is beyond the scope of this work.

#### D. Initial-state, final-state, and the determinant XAS

Lastly, we rationalize the determinant calculation by comparing the determinant spectra with the initial- and final-state spectra (even rows in Fig. 5).

For the 1D tight-binding chain, the MND effects manifest as an asymmetric, power-law singularity that diverges at the absorption edge. Note that this singularity has already been reproduced at the  $f^{(1)}$  level. Thanks to the final-state orbitals in the determinant formalism, one does not need to go over many orders of Feynman diagrams expanded in the initial-state orbitals to produce the edge singularity. The determinant spectrum does not resemble the one-body final-state spectrum, which looks like a “half dome,” making the inclusion of MND effects essential to the spectral calculation. The singularity at 2 eV is the van Hove singularity due to the 1D band edge.

Similar MND effects also manifest in the XAS (polarization vector is 45 deg off-plane) of graphite. After the correction of the determinant approach, the first-peak (around 286 eV, due to  $\pi^*$ ) intensity is significantly magnified compared with the final-state XAS. The corrected intensity ratio of the first peak to the second (around 293 eV) is 1.25 (0.65 in the final-state spectrum), which is in good agreement with 1.35 in a previous experiment [63]. The spectral plateau between 288 and 292 eV (due to the constant joint DOS in 2D systems) is also tilted upward at the low-energy end, due to the MND effects. Such MND effects in graphite were also obtained from first principles using a more complex approach based on Green’s function, which involves energy and time integral, and Fourier transformation [55,56,58]. Here the determinant approach provides equivalent spectra by only a one-shot matrix inversion and a heuristic search of computationally accessible configuration space. It should be noted that both the determinant spectrum in this work and the MND spectrum in Ref. [58] cannot reproduce the splitting of the  $\sigma^*$  peak at 292.5 eV, which could instead be explained by lattice vibrational effects as in a recent work [59].

Significant intensity correction of the peak at onset is also observed in LiCoO<sub>2</sub>, Li, and RuO<sub>3</sub>. In LiCoO<sub>2</sub>, the intensity ratio of the peak at 528 eV to the peak at 532 eV as found by the determinant approach is 2 : 1, which is in good agreement with a previous measurement [64]. In the same work, the intensity ratio by the one-body final-state approach with GGA +  $U$  is 1 : 1, which is consistent with our calculation. In RuO<sub>3</sub>, the intensity ratios of two near-edge peaks are reversed

after correction, which was also reported in our previous work on  $3d$  TMOs [1,2].

The Li  $K$  edge calculated from the determinant formalism (at the level of  $f^{(4)}$ ) for Li metal is in good agreement with a previous experiment [65]. Thermal vibration of the lattice could further modify the spectrum [44], and may broaden the peaks at 61 and 63 eV, making it in closer agreement with the experiment. However, thermal effects will not be discussed in this work, because we focus on the convergence with respect to shakeup orders.

The core-hole attraction effect is most significant in the 1D chain, graphite, and Li, although they are gapless systems. After the inclusion of the core hole, the initial-state spectra dramatically redshift. However, the core-hole effect only causes the initial-state spectra to redshift rigidly in  $\text{LiCoO}_2$ ,  $\text{RuO}_3$ , and Cu. The redshifts of the lowest-energy peaks in  $\text{LiCoO}_2$  and  $\text{RuO}_3$  are 1.28 and 0.34 eV respectively, which are not negligibly small, although the core hole is at the O site where the near-edge orbitals are mainly composed of TM  $d$  orbitals. This explains why initial-state spectra are sometimes good approximation to XAS for O  $K$  edges in TMOs, as discussed in Ref. [3].

### III. CONCLUSIONS

In summary, we have introduced two theorems for regulating the convergence of the determinant calculation, using a SVD analysis over the auxiliary  $\zeta$  matrix. The convergence with respect to the excitation order  $n$  depends on the number of the significant singular values of the  $\zeta$  matrix. We show that the cumulative product of the singular values  $s^1 s^2 \dots s^n$  can be used as an effective estimate for the  $f^{(n)}$  contribution. It is found empirically that it is safe to neglect the  $f^{(n)}$  contribution and higher-order when  $s^1 s^2 \dots s^n < 0.5 \max_m \{s^1 s^2 \dots s^m\}$ . However, satisfactory determinant spectra have been achieved

at the order of  $f^{(2)}$  for all the examined cases (in this work and the TMOs as in Ref. [2]).

### ACKNOWLEDGMENTS

Theoretical and computational work was performed by Y.L. and D.P. at The Molecular Foundry, which is supported by the Office of Science, Office of Basic Energy Sciences, of the United States Department of Energy under Contact No. DE-AC02-05CH11231. Computations were performed with the computing resources at the National Energy Research Scientific Computing Center (NERSC).

### APPENDIX: COMPUTATIONAL DETAILS

The single-body energies and orbitals for both the initial- and final-state systems are obtained with DFT  $\Delta$ SCF calculations, as described in Refs. [1,2]. PBE functionals are used for the DFT calculations. Modified pseudopotentials (by changing  $1s^2$  to  $1s^1$ ) are generated for simulating the core-hole potential of  $K$  edges. We use exactly the same set of pseudopotentials for all the atoms in initial-state and final-state calculations, except for the core-excited atom. Supercell dimensions are chosen to be approximately  $10 \text{ \AA}$  that is sufficient to minimize spurious periodic interactions among the core-hole impurities. The  $\Delta$ SCF calculations for TMOs are performed using the DFT+ $U$  theory [15] with the  $U$  value adopted from Ref. [17]. A  $5 \times 5 \times 5$   $k$  grid is used to sample the BZ of the supercell, which is essential for high-energy scattering states and metallic systems. The DFT part of the calculations is performed using a local repository of the ShirleyXAS code, which is available at the David Prendergast's group at the Molecular Foundry.

The determinant calculations are performed using an open source software package, MBXASPY, which is available at [67].

- 
- [1] Y. Liang, J. Vinson, S. Pemmaraju, W. S. Drisdell, E. L. Shirley, and D. Prendergast, Accurate X-Ray Spectral Predictions: An Advanced Self-Consistent-Field Approach Inspired by Many-Body Perturbation Theory, *Phys. Rev. Lett.* **118**, 096402 (2017).
- [2] Y. Liang and D. Prendergast, Quantum many-body effects in x-ray spectra efficiently computed using a basic graph algorithm, *Phys. Rev. B* **97**, 205127 (2018).
- [3] F. De Groot and A. Kotani, *Core Level Spectroscopy of Solids* (CRC, Boca Raton, FL, 2008).
- [4] C. S. Fadley, X-ray photoelectron spectroscopy: Progress and perspectives, *J. Electron Spectrosc. Relat. Phenom.* **178**, 2 (2010).
- [5] J. Singh, C. Lamberti, and J. A. van Bokhoven, Advanced x-ray absorption and emission spectroscopy: In situ catalytic studies, *Chem. Soc. Rev.* **39**, 4754 (2010).
- [6] L. J. Ament, M. Van Veenendaal, T. P. Devereaux, J. P. Hill, and J. Van Den Brink, Resonant inelastic x-ray scattering studies of elementary excitations, *Rev. Mod. Phys.* **83**, 705 (2011).
- [7] J. A. Van Bokhoven and C. Lamberti, *X-ray Absorption and X-ray Emission Spectroscopy: Theory and Applications* (John Wiley & Sons, New York, 2016).
- [8] P. Emma, R. Akre, J. Arthur, R. Bionta, C. Bostedt, J. Bozek, A. Brachmann, P. Bucksbaum, R. Coffee, F. J. Decker *et al.*, First lasing and operation of an ångstrom-wavelength free-electron laser, *Nat. Photon.* **4**, 641 (2010).
- [9] W. F. Schlotter, J. J. Turner, M. Rowen, P. Heimann, M. Holmes, O. Krupin, M. Messerschmidt, S. Moeller, J. Krzywinski, R. Soufli *et al.*, The soft x-ray instrument for materials studies at the linac coherent light source x-ray free-electron laser, *Rev. Sci. Instrum.* **83**, 043107 (2012).
- [10] H. T. Lemke, C. Bressler, L. X. Chen, D. M. Fritz, K. J. Gaffney, A. Galler, W. Gawelda, K. Haldrup, R. W. Hartsock, H. Ihee *et al.*, Femtosecond x-ray absorption spectroscopy at a hard x-ray free electron laser: Application to spin crossover dynamics, *J. Phys. Chem. A* **117**, 735 (2013).
- [11] D. Prendergast and G. Galli, X-Ray Absorption Spectra of Water from First Principles Calculations, *Phys. Rev. Lett.* **96**, 215502 (2006).
- [12] D. Cabaret, A. Bordage, A. Juhin, M. Arfaoui, and E. Gaudry, First-principles calculations of x-ray absorption spectra at the K-edge of 3d transition metals: An electronic structure analysis of the pre-edge, *Phys. Chem. Chem. Phys.* **12**, 5619 (2010).

- [13] C. Gougoussis, M. Calandra, A. P. Seitsonen, and F. Mauri, First-principles calculations of x-ray absorption in a scheme based on ultrasoft pseudopotentials: From  $\alpha$ -quartz to high- $T_c$  compounds, *Phys. Rev. B* **80**, 075102 (2009).
- [14] R. G. Parr, *Density Functional Theory of Atoms and Molecules* (Springer, Berlin, 1980), pp. 5–15.
- [15] S. L. Dudarev, G. A. Botton, S. Y. Savrasov, C. J. Humphreys, and A. P. Sutton, Electron-energy-loss spectra and the structural stability of nickel oxide: An LSDA+ $U$  study, *Phys. Rev. B* **57**, 1505 (1998).
- [16] F. M. Bickelhaupt, and E. J. Baerends, Kohn-Sham density functional theory: Predicting and understanding chemistry, *Rev. Comp. Chem.* **15**, 1 (2000).
- [17] L. Wang, T. Maxisch, and G. Ceder, Oxidation energies of transition metal oxides within the GGA+ $U$  framework, *Phys. Rev. B* **73**, 195107 (2006).
- [18] G. Hautier, S. P. Ong, A. Jain, C. J. Moore, and G. Ceder, Accuracy of density functional theory in predicting formation energies of ternary oxides from binary oxides and its implication on phase stability, *Phys. Rev. B* **85**, 155208 (2012).
- [19] C. T. Chen, F. Sette, Y. Ma, M. S. Hybertsen, E. B. Stechel, W. M. C. Foulkes, M. Schulter, S. W. Cheong, A. S. Cooper, and L. W. Rupp, Jr. *et al.*, Electronic States in  $\text{La}_{2-x}\text{Sr}_x\text{CuO}_{4+\delta}$  Probed by Soft-X-Ray Absorption, *Phys. Rev. Lett.* **66**, 104 (1991).
- [20] M. S. Hybertsen, E. B. Stechel, W. M. C. Foulkes, and M. Schlüter, Model for low-energy electronic states probed by x-ray absorption in high- $T_c$  cuprates, *Phys. Rev. B* **45**, 10032 (1992).
- [21] M. W. Haverkort, M. Zwierzycki, and O. K. Andersen, Multiplet ligand-field theory using Wannier orbitals, *Phys. Rev. B* **85**, 165113 (2012).
- [22] S. Kourtis, J. van den Brink, and M. Daghofer, Exact diagonalization results for resonant inelastic x-ray scattering spectra of one-dimensional Mott insulators, *Phys. Rev. B* **85**, 064423 (2012).
- [23] A. Uldry, F. Vernay, and B. Delley, Systematic computation of crystal-field multiplets for x-ray core spectroscopies, *Phys. Rev. B* **85**, 125133 (2012).
- [24] C. C. Chen, M. Sentef, Y. F. Kung, C. J. Jia, R. Thomale, B. Moritz, A. P. Kampf, and T. P. Devereaux, Doping evolution of the oxygen  $K$ -edge x-ray absorption spectra of cuprate superconductors using a three-orbital Hubbard model, *Phys. Rev. B* **87**, 165144 (2013).
- [25] C. Jia, K. Wohlfeld, Y. Wang, B. Moritz, and T. P. Devereaux, Using RIXS to Uncover Elementary Charge and Spin Excitations, *Phys. Rev. X* **6**, 021020 (2016).
- [26] Y. Lu and M. W. Haverkort, Nonperturbative Series Expansion of Green's Functions: The Anatomy of Resonant Inelastic X-Ray Scattering in the Doped Hubbard Model, *Phys. Rev. Lett.* **119**, 256401 (2017).
- [27] C. D. Sherrill, H. F. Schaefer, III, *The Configuration Interaction Method: Advances in Highly Correlated Approaches* (Elsevier, Amsterdam, 1999), pp. 143–269.
- [28] N. M. Tubman, J. Lee, T. Y. Takeshita, M. Head-Gordon, and K. B. Whaley, A deterministic alternative to the full configuration interaction quantum Monte Carlo method, *J. Chem. Phys.* **145**, 044112 (2016).
- [29] R. J. Bartlett and M. Musiał, Coupled-cluster theory in quantum chemistry, *Rev. Mod. Phys.* **79**, 291 (2007).
- [30] P. G. Szalay, T. Muller, G. Gidofalvi, H. Lischka, and R. Shepard, Multiconfiguration self-consistent field and multireference configuration interaction methods and applications, *Chem. Rev.* **112**, 108 (2011).
- [31] M. Roemelt and F. Neese, Excited states of large open-shell molecules: An efficient, general, and spin-adapted approach based on a restricted open-shell ground state wave function, *J. Phys. Chem. A* **117**, 3069 (2013).
- [32] R. V. Pinjari, M. G. Delcey, M. Guo, M. Odelius, and M. Lundberg, Restricted active space calculations of L-edge X-ray absorption spectra: From molecular orbitals to multiplet states, *J. Chem. Phys.* **141**, 124116 (2014).
- [33] D. Maganas, S. DeBeer, and F. Neese, A restricted open configuration interaction with singles method to calculate valence-to-core resonant x-ray emission spectra: A case study, *Inorg. Chem.* **56**, 11819 (2017).
- [34] M. Nyberg, Y. Luo, L. Triguero, L. G. Pettersson, and H. Ågren, Core-hole effects in x-ray-absorption spectra of fullerenes, *Phys. Rev. B* **60**, 7956 (1999).
- [35] M. Taillefumier, D. Cabaret, A. Flank, and F. Mauri, X-ray absorption near-edge structure calculations with the pseudopotentials: Application to the  $K$  edge in diamond and  $\alpha$ -quartz, *Phys. Rev. B* **66**, 195107 (2002).
- [36] E. L. Shirley, *Ab Initio* Inclusion of Electron-Hole Attraction: Application to X-Ray Absorption and Resonant Inelastic X-Ray Scattering, *Phys. Rev. Lett.* **80**, 794 (1998).
- [37] W. Olovsson, I. Tanaka, T. Mizoguchi, P. Puschnig, and C. Ambrosch-Draxl, All-electron Bethe-Salpeter calculations for shallow-core x-ray absorption near-edge structures, *Phys. Rev. B* **79**, 041102(R) (2009).
- [38] J. Vinson, J. J. Rehr, J. J. Kas, and E. L. Shirley, Bethe-Salpeter equation calculations of core excitation spectra, *Phys. Rev. B* **83**, 115106 (2011).
- [39] N. A. Besley, M. J. Peach, and D. J. Tozer, Time-dependent density functional theory calculations of near-edge x-ray absorption fine structure with short-range corrected functionals, *Phys. Chem. Chem. Phys.* **11**, 10350 (2009).
- [40] N. A. Besley and F. A. Asmuruf, Time-dependent density functional theory calculations of the spectroscopy of core electrons, *Phys. Chem. Chem. Phys.* **12**, 12024 (2010).
- [41] K. Lopata, B. E. Van Kuiken, M. Khalil, and N. Govind, Linear-response and real-time time-dependent density functional theory studies of core-level near-edge x-ray absorption, *J. Chem. Theory Computation* **8**, 3284 (2012).
- [42] C. D. Pemmaraju, F. D. Vila, J. J. Kas, S. A. Sato, J. J. Rehr, K. Yabana, and D. Prendergast, Velocity-gauge real-time TDDFT within a numerical atomic orbital basis set, *Comput. Phys. Commun.* **226**, 30 (2018).
- [43] Y. Zhang, J. D. Biggs, D. Healion, N. Govind, and S. Mukamel, Core and valence excitations in resonant x-ray spectroscopy using restricted excitation window time-dependent density functional theory, *J. Chem. Phys.* **137**, 194306 (2012).
- [44] T. A. Pascal, U. Boesenberg, R. Kostecki, T. J. Richardson, T. Weng, D. Sokaras, D. Nordlund, E. McDermott, A. Moewes, J. Cabana *et al.*, Finite temperature effects on the x-ray absorption spectra of lithium compounds: First-principles interpretation of x-ray Raman measurements, *J. Chem. Phys.* **140**, 034107 (2014).
- [45] J. Velasco-Velez, C. H. Wu, T. A. Pascal, L. F. Wan, J. Guo, D. Prendergast, and M. Salmeron, The structure of interfacial water

- on gold electrodes studied by x-ray absorption spectroscopy, *Science* **346**, 831 (2014).
- [46] C. Zhan, Z. Yao, J. Lu, L. Ma, V. A. Maroni, L. Li, E. Lee, E. E. Alp, T. Wu, J. Wen *et al.*, Enabling the high capacity of lithium-rich anti-fluorite lithium iron oxide by simultaneous anionic and cationic redox, *Nat. Energy* **2**, 963 (2017).
- [47] G. D. Mahan, Excitons in Metals, *Phys. Rev. Lett.* **18**, 448 (1967).
- [48] P. Nozieres and C. T. De Dominicis, Singularities in the x-ray absorption and emission of metals. III. One-body theory exact solution, *Phys. Rev.* **178**, 1097 (1969).
- [49] K. Ohtaka and Y. Tanabe, Theory of the soft-x-ray edge problem in simple metals: historical survey and recent developments, *Rev. Mod. Phys.* **62**, 929 (1990).
- [50] G. D. Mahan, *Many-Particle Physics*, Springer Science & Business Media (Springer, New York, 2013).
- [51] P. W. Anderson, Infrared Catastrophe in Fermi Gases with Local Scattering Potentials, *Phys. Rev. Lett.* **18**, 1049 (1967).
- [52] K. S. Kim, X-ray-photoelectron spectroscopic studies of the electronic structure of CoO, *Phys. Rev. B* **11**, 2177 (1975).
- [53] E. A. Stern and J. J. Rehr, Many-body aspects of the near-edge structure in x-ray absorption, *Phys. Rev. B* **27**, 3351 (1983).
- [54] M. Calandra, J. P. Rueff, C. Gougoussis, D. Céolin, M. Gorgoi, S. Benedetti, P. Torelli, A. Shukla, D. Chandesris, and C. Brouder, *K*-edge x-ray absorption spectra in transition-metal oxides beyond the single-particle approximation: Shake-up many-body effects, *Phys. Rev. B* **86**, 165102 (2012).
- [55] O. Wessely, M. I. Katsnelson, and O. Eriksson, *Ab Initio* Theory of Dynamical Core-Hole Screening in Graphite from X-Ray Absorption Spectra, *Phys. Rev. Lett.* **94**, 167401 (2005).
- [56] O. Wessely, O. Eriksson, and M. I. Katsnelson, Dynamical core-hole screening in the x-ray absorption spectra of graphite, C60, and carbon nanotubes: A first-principles electronic structure study, *Phys. Rev. B* **73**, 075402 (2006).
- [57] O. Wessely, M. I. Katsnelson, A. Nilsson, A. Nikitin, H. Ogasawara, M. Odelius, B. Sanyal, and O. Eriksson, Dynamical core-hole screening in the x-ray absorption spectra of hydrogenated carbon nanotubes and graphene, *Phys. Rev. B* **76**, 161402(R) (2007).
- [58] R. E. Ovcharenko, I. I. Tupitsyn, E. P. Savinov, E. N. Voloshina, B. Paulus, Y. S. Dedkov, and A. S. Shulakov, Specific many-electron effects in x-ray spectra of simple metals and graphene, *Phys. Chem. Chem. Phys.* **15**, 6749 (2013).
- [59] W. Olovsson, T. Mizoguchi, M. Magnuson, S. Kontur, O. Hellman, I. Tanaka, and C. Draxl, Vibrational effects in x-ray absorption spectra of two-dimensional layered materials, *J. Phys. Chem. C* **123**, 9688 (2019).
- [60] G. Vidal, Classical Simulation of Infinite-Size Quantum Lattice Systems in One Spatial Dimension, *Phys. Rev. Lett.* **98**, 070201 (2007).
- [61] H. Li and F. D. M. Haldane, Entanglement Spectrum as a Generalization of Entanglement Entropy: Identification of Topological Order in Non-Abelian Fractional Quantum Hall Effect States, *Phys. Rev. Lett.* **101**, 010504 (2008).
- [62] U. Schollwöck, The density-matrix renormalization group in the age of matrix product states, *Ann. Phys.* **326**, 96 (2011).
- [63] M. Weser, Y. Rehder, K. Horn, M. Sicot, M. Fonin, A. B. Preobrajenski, E. N. Voloshina, E. Goering, and Yu. S. Dedkov, Induced magnetism of carbon atoms at the graphene/Ni(111) interface, *Appl. Phys. Lett.* **96**, 012504 (2010).
- [64] A. Juhin, F. de Groot, G. Vankó, M. Calandra, and C. Brouder, Angular dependence of core hole screening in LiCoO<sub>2</sub>: A DFT+*U* calculation of the oxygen and cobalt *K*-edge x-ray absorption spectra, *Phys. Rev. B* **81**, 115115 (2010).
- [65] P. S. Miedema, P. Ngene, A. M. J. van der Eerden, D. Sokaras, T. C. Weng, D. Nordlund, Y. S. Aua, and F. M. F. de Groot, In situ x-ray Raman spectroscopy study of the hydrogen sorption properties of lithium borohydride nanocomposites, *Phys. Chem. Chem. Phys.* **16**, 22651 (2014).
- [66] L. S. Kau, K. O. Hodgson, and E. I. Solomon, X-ray absorption edge and EXAFS study of the copper sites in zinc oxide methanol synthesis catalysts, *J. Am. Chem. Soc.* **111**, 7103 (1989).
- [67] <https://github.com/yufengliang/mbxaspy>.